Mixing gases into medium-consistency pulp suspensions using rotary devices

Chad P. J. Bennington

ABSTRACT: The conditions under which gases can be effectively mixed into medium-consistency pulp suspensions were determined in the laboratory using a shear tester similar in design to commercial pulp mixers. Mixing effectiveness was evaluated based on (a) the flow pattern observed with a high-speed video system and (b) the power drawn in mixing. For Newtonian fluids and air/water dispersions, mixing was similar to that of conventional stirred vessel mixers. For medium-consistency pulp suspensions, the gas-mixing ability was markedly reduced. For example, the mixing power (compared with water) was reduced by 50% when the void fraction reached 120% of the volume between the rotor lugs. This limited the volume of gas that could be effectively mixed into the suspension and was attributed to the rotor being unable to transfer shear and momentum to the suspension.

KEYWORDS: Dispersions, gas, medium consistency, mixing, pulps.

Pulp fiber processing is commonly carried out in the medium-consistency range where the mass concentration of the suspension, C_m, is between 0.08 and 0.16. In pulp bleaching operations we must often mix gaseous reagents into these suspensions. Current bleaching practice makes extensive use of gaseous chlorine and oxygen, and the use of ozone is under development. When mixed with the suspension, these gases can make up a substantial portion of the suspension volume. For example, a $C_m = 0.12$ softwood kraft suspension reacted under typical oxygen bleaching conditions (2.2% O_2 on pulp by mass at an operating pressure of 750 kPa and temperature of 100°C) would have an initial gas volume of approximately 26%. Other typical suspension gas contents encountered in common bleaching operations are given in **Table I**.

When gases are mixed into pulp suspensions, it is important to achieve good mixing over the macroscale, fiber-scale, and microscale. This ensures the uniform distribution of reagents throughout the suspension and leads to uniform bleaching. In order to achieve this, the gas phase must not impair the suspension flow or the operation of the mixer. Effective bleaching also requires that the interfacial area of the gas phase be maximized to improve mass transfer and chemical reaction, and that a mixed state be maintained upon exiting the mixer to facilitate uniform bleaching in the retention tower.

Past studies concerning the mixing of pulp fiber suspensions have been summarized by Bennington, Kerekes, and Grace (*1*). Only a few investigations have addressed suspension mixing at medium consistencies, and no study directly examined the mixing of gases into these suspensions. The work on medium-consistency pulp rheology by Gullichsen and Harkonen (*2*) identified the conditions under which fluid-like motion could be induced in the suspensions, enabling transport by centrifugal pumps and mixing in a turbulent manner. Later work by Bennington, Kerekes, and Grace (*3, 4*) demonstrated the range of flow regimes that could be created in a mixing vessel and the role played by the suspension yield stress. In their con-

Bennington is a research engineer with the Pulp and Paper Research Institute of Canada and an adjunct professor in the Department of Chemical Engineering at the University of British Columbia. He is located at the Pulp and Paper Centre, 2385 East Mall, Vancouver, BC, V6T 1Z4, Canada.

I. Pulp suspension gas content under typical bleaching conditions

Operating conditions	*Pulp mass concentration, C_m fraction*	*Operating pressure (absolute), kPa*	*Operating temp., °C*	*Gas phase added, fraction*	*Gas phase after saturation of water,[a] fraction*
Air content of kraft pulp *(12)*	0.10	100	25	-	0.10
Chlorination of 30 kappa kraft pulp (7.2% active chlorine on pulp)					
C_{100}	0.03	350	30	0.18	0.0
C_{100}	0.12	350	50	0.49	0.0
$C_{50}D_{50}$	0.12	350	50	0.32	0.0
Oxygen delignification of kraft pulp. O_2 = 2.2% by mass	0.12	750	100	0.26	0.25
Oxidative extraction (E_o) O_2 = 0.5% by mass	0.12	450	70	0.11	0.09
Ozone bleaching[b] 1% O_3 on pulp, 7% O_3 in O_2	0.10	700	70	0.64	0.64

Assumptions: gas contents are calculated for initial contacting conditions prior to chemical reaction.
[a]All suspension water is assumed to be available to dissolve the gas phase, including water inside the swollen pulp fibers.
[b]Ozone bleaching is in development. Potential bleaching conditions obtained from the 1991 International Pulp Bleaching Conference, Stockholm, Sweden.

centric-cylinder apparatus, they identified two regimes, termed "cellular flow" and "outward radial flow" that resulted in macroscale and fiber-scale mixing of the vessel contents. The ability of the suspension gas content to prevent complete motion in the device was noted but not systematically investigated.

The present study examines the effect of gas content on the flow behavior and mixing of medium-consistency pulp suspensions in a batch-operated rotary shear tester. The mixing device chosen had a concentric-cylinder geometry, consisting of a vaned rotor and baffled housing, and was similar in design to commercial and laboratory pulp mixers.

Experimental

The batch-operated concentric-cylinder shear tester used in this study is illustrated in **Fig. 1.** The device is powered by a 22.4-kW dc motor and is capable of static torques of 85 N·m and rotational speeds of up to 83 s^{-1}. The pulp suspensions are placed in the

1. Side view of the rotary shear tester. (1) 22.4-kW dc motor; (2) toothed drive belt; (3) instrumented main shaft; (4) concentric-cylinder chamber comprising lugged rotor and baffled housing.

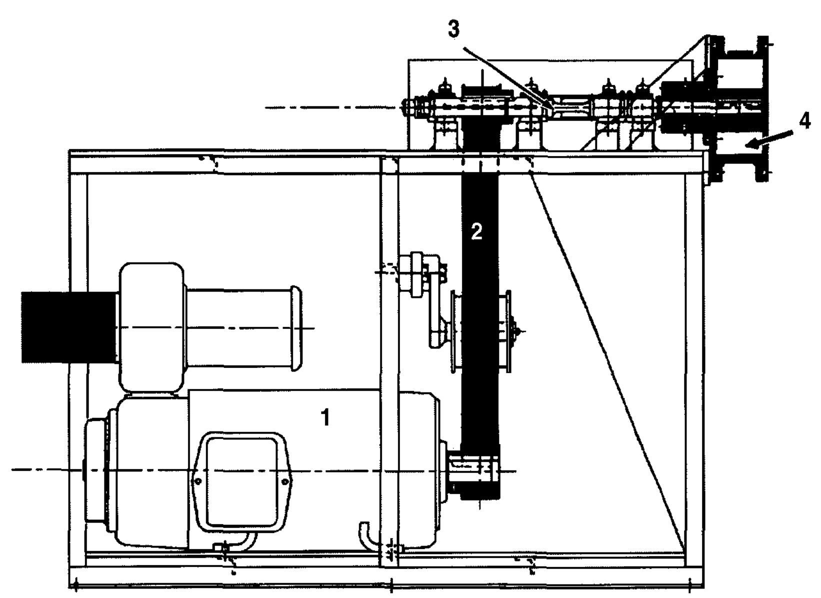

2. Rotor and housing configurations used in tests. Dimensions are in millimeters. (a) Rotor A, (b) Rotor B.

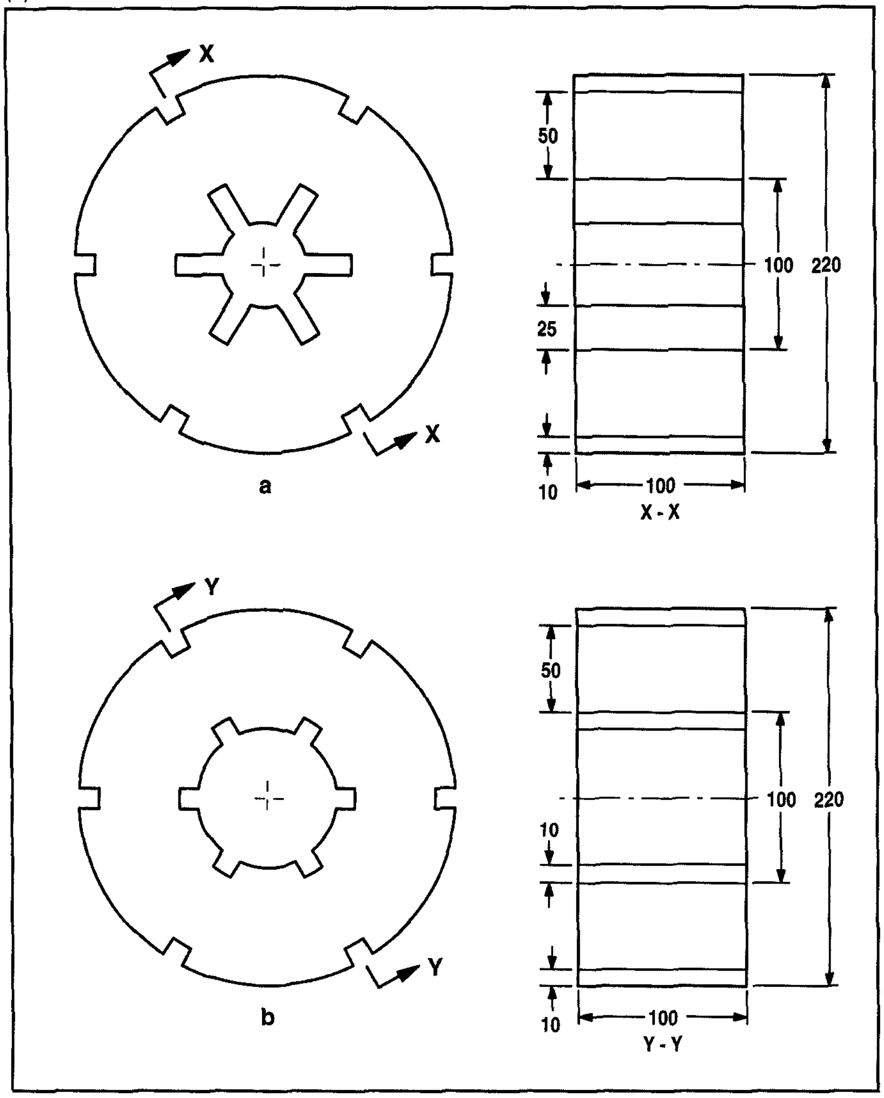

chamber formed between the outer housing baffled at 60 degree intervals and an inner lugged rotor. Two rotor geometries were studied and are illustrated in **Fig. 2.** The outer dimensions of the rotors are identical—only the volume between the rotor vanes differed. The baffles and lugs were necessary to impose as much of a no-slip condition between the rotor surfaces and the fiber suspensions as possible. The suspension would otherwise slip over smooth surfaces due to its yield strength and solid-like properties. The chamber is enclosed with a transparent Lexan plate, which permitted observation and photography of the flows.

The rotary shear tester was first characterized using Newtonian fluids of different viscosity [water, water/glycerol solutions, Shell Omala 1000 (a paraffinic hydrocarbon lubricant), and Dow Corning 200 Fluid (a dimethyl siloxane polymer)]. Fluid viscosities were measured using a Haake RV12 viscometer or obtained from data supplied by the manufacturers. Gas tests were conducted with water, with the void fraction of air ranging from 0 to 0.75. Gas bubble sizes were determined by measuring the bubble diameters from photographs taken of the dispersions.

Medium-consistency pulp suspension tests were conducted using a commercial, fully bleached softwood kraft pulp (FBK). The pulp had been dried in sheet form and was reslurried in a British standard disintegrator prior to being made into suspensions of known mass concentration. Measured masses of suspension at chosen mass concentrations were added to the test chamber to give gas-phase contents, X_g, of between 0 and 0.20, calculated using Eq. 1:

$$X_g = 1 - \{(C_m/\rho_f) + [(1 - C_m)/\rho_w]\}\rho_b \qquad (1)$$

where

ρ_f = 1500 kg/m^3, density of cellulose

ρ_w = density of water

ρ_b = bulk density of the suspension (determined by dividing the mass of pulp tested, m_T, by the total volume of the mixing vessel, V_T).

C_m = mass concentration of the suspension (expressed as a fraction)

Two test methods were used. In the first type, an impeller rotational speed was set and allowed to stabilize before torque readings were obtained. In the second, the torque was measured at 0.04 s intervals as the rotational speed was increased at a constant rate from rest to 83 s^{-1} in 25 s. All data were corrected for bearing friction, which was measured by running the shear tester in air. Flash photographs and video images obtained with a Kodak Ekta-Pro 1000 video system were used to study flow profiles and gas dispersion.

Characterization of shear tester using Newtonian fluids

The rotary shear tester is essentially a batch-operated, fully-baffled mixer having a rotor design similar to that of a Rushton turbine. In such devices, macroscale mixing is governed by bulk flow, while microscale mixing is governed by the shear and energy dissipation within the vessel. As both are linked with the power drawn in mixing, it is common to utilize data that relate mixing power to operating conditions for both the design and evaluation of mixers.

3. Power number vs. Reynolds number for Rotors A (Δ) and B (□) with Newtonian fluids under non-gassed conditions

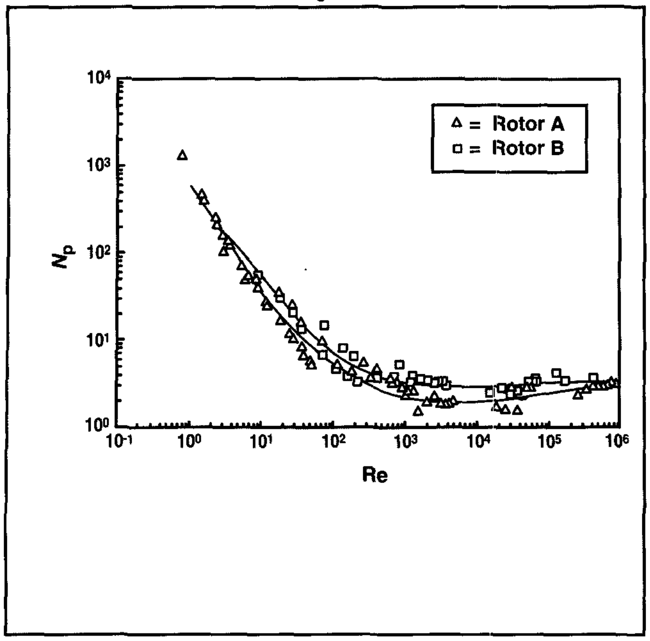

4. Gassed power ratio (P_g/P_o) vs. gas content (X_g) for Rotor A (air/water mixtures)

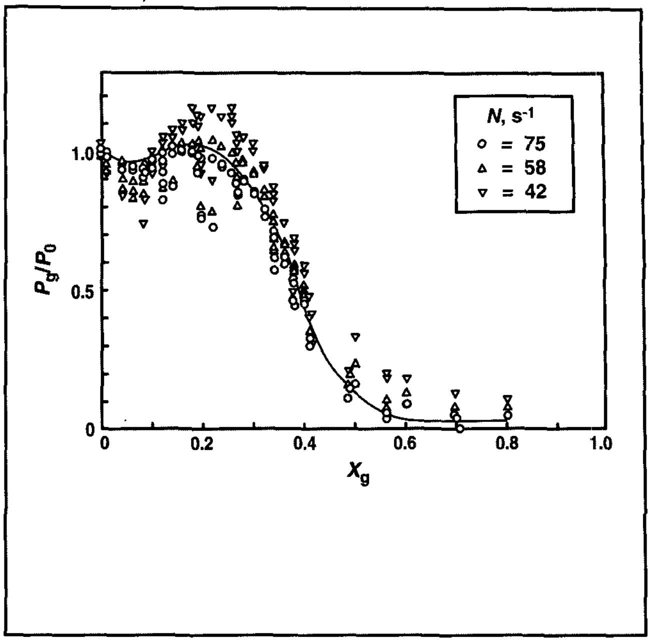

The operation of the rotary shear tester was characterized with Newtonian fluids, and the results are given by power curves in **Fig. 3**. Above a Reynolds number of approximately 300, the shear tester operated in a turbulent regime with the impeller power number being reasonably constant. This is consistent with results obtained for standard fluid mixers by Gray (*5*) and Nagata (*6*).

The addition of gas to the mixing chamber reduces the power drawn by the impeller. The ratio of the mixing power drawn under conditions where gas is present to that drawn in the absence of gas, P_g/P_o, is termed the gassed power ratio and is used to characterize mixer performance in the presence of a gas phase. The gassed power ratio measured for air/water dispersions is plotted against the gas void fraction in **Figs. 4** and **5** for Rotors A and B, respectively. Note that the data given are only for rotor speeds greater than 42 s^{-1}. When the rotor speed was reduced below this value, the uncertainty in measuring the torque (± 0.3 N·m) resulted in unacceptably high errors when calculating P_g/P_o. This can be illustrated by examining some representative data. For example, we find that for Rotor A with X_g =0.39 at 75 s^{-1}, P_g/P_o =0.33 ± 0.03, an uncertainty of 8.3%. At 42 s^{-1}, however, we obtain P_g/P_o =0.48 ± 0.12, an uncertainty of 24%.

For Rotor A (Fig. 4) $P_g/P_o \approx 1$ at gas contents below X_g =0.2. Above X_g =0.2, P_g/P_o decreased steadily as gas content was increased. No power was drawn when the liquid level was below the rotor. The bulk-flow pattern of the dispersion exhibited either an outward radial flow of fluid or an inward radial flow of fluid. The latter regime was called the cellular flow regime (*4*), as it formed six cells that corresponded to the six baffles on the outer housing. The solid line drawn through the points in Fig. 4 represents the gassed power curve when both the dispersion and the reference (ungassed) tests were in the cellular regime. For the data obtained at a rotor speed of N =42 s^{-1}, P_g/P_o can reach values as high as 1.15. In this case, the dispersion is in the cellular flow regime, and the reference ungassed state is in outward radial flow. Those points below the line have the dispersed flow in the outward radial flow regime and the ungassed flow in the cellular regime. This indicates that maintenance of cellular flow requires more power than outward radial flow.

II. Bubble diameter versus energy input. Air/water system. X_g = 0.19.

N, s^{-1}	ε_m, m^2/s^3	Bubble diameter, mm: Measured d_{10}	Measured d_{32}	Calculated (9) d_{max}
8.3	3.8	2.3	3.6	1.36
17	38	1.2	1.7	0.54
25	150	0.6	0.8	0.31
33	370	0.5	0.6	0.22
50	1.2×10^3	0.3	0.4	0.14
83	4.3×10^3	<0.2	0.2	0.08

For Rotor B (Fig. 5) two curves are plotted. The first shows a steady decrease in P_g/P_o with gas content down to $X_g \approx$ 0.3. This curve represents the case where the dispersion is in outward radial flow. The second curve begins at X_g =0.2, decreases steadily with increasing gas content, and corresponds to the case where the dispersion is in cellular flow. This latter curve corresponds closely with that found for Rotor A. Note that the two curves for Rotor B overlap when X_g is between approximately 0.2 and 0.3 indicating that both flow regimes are possible within this range of gas content.

5. Gassed power ratio (P_g/P_o) vs. gas content (X_g) for Rotor B (air/water mixtures)

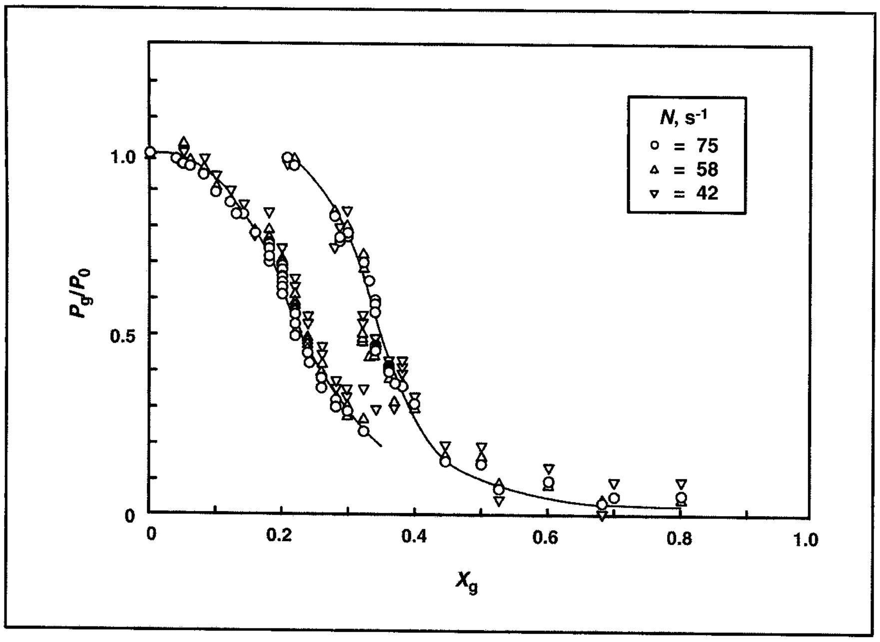

6. Reduction in air bubble size with increased rotor speed (air/water mixture, X_g =0.19). (a) N=8.3 s^{-1}, d_{10} =2.3 mm; (b) N=25 s^{-1}, d_{10} =0.6 mm; (c) N =50 s^{-1}, d_{10} =0.3 mm.

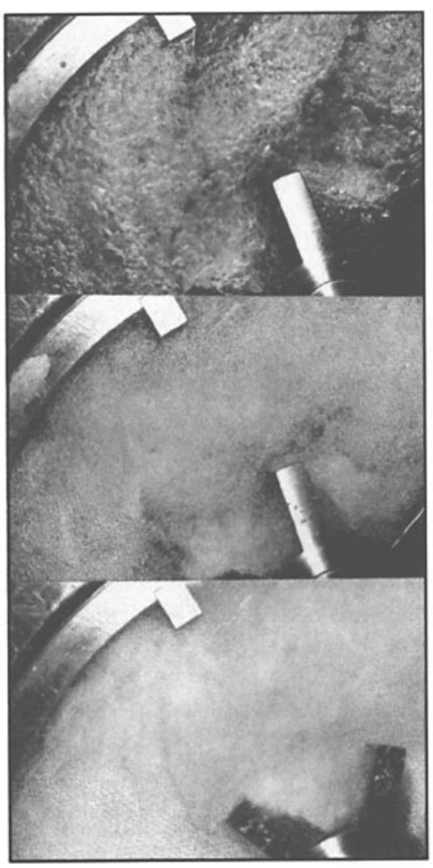

The reduction in impeller power when gas is present has been attributed to the streamlining effect of stable gas cavities which form behind the rotor lugs (*7*). As the gas fraction is increased, the gas cavities enlarge and reduce the area available for liquid outflow. This results in a corresponding drop in the pumping capacity of the rotor and a decrease in the power drawn by the impeller. The existence of different flow patterns in agitated vessels has usually been noted only in conjunction with viscoelastic fluids. However, Ando, Hara, and Endoh (*8*) noted a hysteresis loop in torque accompanied by changes in flow pattern as impeller rotational speed was changed in a horizontally stirred vessel. Both impeller power and flow hydrodynamics are important in determining mixing. This is particularly true for gas/liquid contacting where both phases should be well mixed.

The gas phase exists as a bubbly dispersion in the air/water tests. The interfacial area increases (the mean bubble diameter decreases) as the impeller rotational speed increases, as shown in **Table II** and illustrated in **Fig. 6** for an air/water dispersion having X_g =0.19. Here, the mean bubble size decreased from 2.3 mm to a cloud of tiny bubbles having an average diameter less than 0.2 mm when the rotor speed was increased from N =8.3 s^{-1} to 83 s^{-1}. The trend exhibited by the data is similar to that predicted by Hinze (*9*), with the bubble diameter decreasing as $\varepsilon_m^{0.37}$. The bubbles appear uniformly dispersed throughout the mixer volume, indicating that the gas phase should be well mixed.

These data demonstrate that the mixing behavior of the shear tester with Newtonian fluids and air/water dispersions is consistent with that of conventional mixers. Having characterized the shear tester by mixing with Newtonian fluids, the mixing of gases with non-Newtonian pulp fiber suspensions will be explored.

Mixing gas into pulp suspensions

The mixing of gas into pulp fiber suspensions was evaluated using two criteria: the bulk flow pattern produced and the power drawn in mixing. The bulk motion was used to indicate operating conditions capable of achieving macroscale mixing, while the power dissipation was used to indicate the shear and turbulence produced within the suspension and thus the level of fiber-scale and microscale mixing. Due to the significant yield stress exhibited by pulp fiber suspensions, both criteria must be utilized simultaneously to ascertain if acceptable gas mixing is possible.

Flow regimes

Bulk suspension flow was observed through the front face of the shear tester. Tests were conducted with Rotor A in which both the mass concentration ($0.06 \leq C_m \leq 0.14$) and gas content ($0.0 \leq X_g \leq 0.20$) of the suspension were varied. A total of six distinct flow regimes were identified, four of which had been observed previously for Rotor B at low suspension gas contents ($X_g \leq 0.03$) (*4*). The flow regimes and their mixing characteristics are described below and illustrated in **Fig. 7**. The regimes identified previously were:

"Couette-like": After the suspension yielded, the fibers and fiber bundles (flocs) adjacent to the rotor moved tangentially with the rotor. At relatively low rotor speeds, suspension motion was confined to an active zone or cavity between the rotor and stagnant suspension. As the rotor speed was increased, the region of motion grew radially outward. Gas within the growing cavity moved to the center of the shear tester and accumulated around the rotor. Depending on the volume of gas present, momentum transfer and thus flow development could be inhibited. In extreme cases, a flooded situation was created. A strong radial gradient in fiber motion was observed in the cavity, as reported previously (*4*).

Outward radial flow: This pattern involved radial outflow from the rotor toward the housing. The entire contents of the vessel were in motion; however, some gas-phase segregation was observed to occur. This flow pattern had been previously observed with Rotor B at low suspension concentrations ($C_m \leq 0.04$) and was believed to be an inversion of the cellular flow pattern (*10*).

Cellular flow: This flow pattern was stable up to the highest rotational speed achieved in the shear tester (83 s^{-1}). Radial inward flow filled the vessel and formed six cells attributed to the six baffles on the housing. The microscale and fiber-scale mixing produced by this flow regime were found from tracer tests to be good (*10*). The gas phase was uniformly distributed within the suspension under most conditions.

Flooding: If sufficient gas accumulated around the rotor, the rotor lugs were unable to shear or transfer momentum to the suspension. Suspension flow stopped, although the rotor continued to turn in the gas pocket it had created. If the quantity of gas was insufficient to completely flood the rotor reduced motion persisted in the vessel, often the "Couette-like" tangential motion described earlier. Even when bulk suspension motion ceased, a torque that represented the frictional resistance of the suspension plug against the rotor was recorded.

7. Flow regimes observed in tests with Rotor A (rotor rotation is counter clockwise). (a) "Couette-like" flow: tangential motion outward to a boundary of stagnant suspension; (b) partial inward radial flow: inward radial flow from a point 1–3 cm from the housing wall; (c) outward radial flow: radial outflow filling the entire vessel; (d) pulsing flow: a region of suspension motion sweeping around the vessel; (e) cellular flow: inward radial flow filling the vessel displaying sixfold symmetry; (f) flooding: the accumulation of sufficient gas around the rotor to inhibit suspension motion.

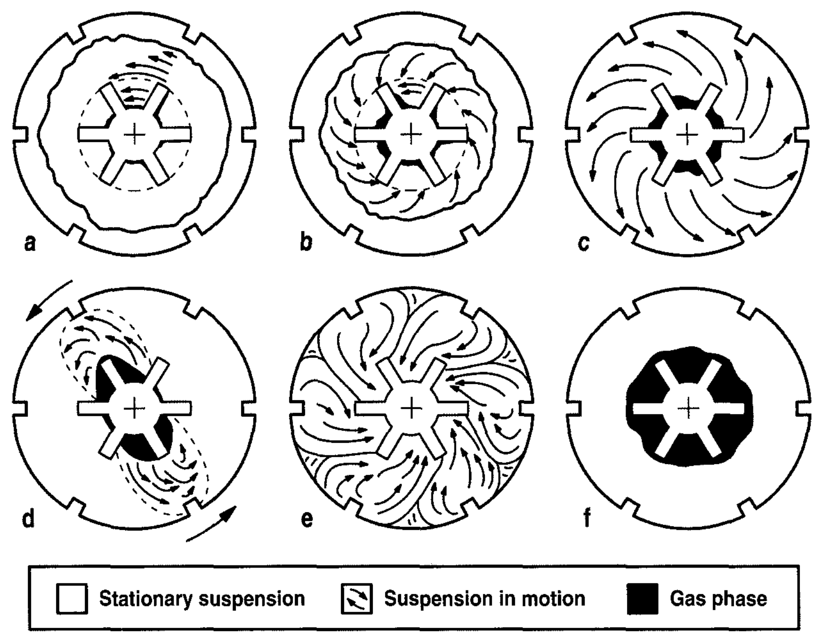

Two new regimes also were identified in this study:

Partial inward radial flow: This flow was observed when the "Couette-like" flow had almost filled the vessel chamber. From the front of the shear tester, the flow involved radial flow inward from a point 1–3 cm from the edge of the housing, thus leaving a ring of stagnant suspension at the periphery of the vessel. The dead zones at the periphery of the vessel would result in poor macroscale mixing.

Pulsing flow: A number of flow patterns were termed "pulsing flow" as they all possessed an intermittent or pulsing quality. In some instances, the suspension would adopt a cellular-type flow, often in one area of the chamber, only to cease flow in that particular area and begin flow in another area. In other instances, a more vigorous region of suspension motion would sweep around the test chamber at a rate significantly lower than that of the rotor. The gas that had accumulated at the eye of the rotor would rotate at the same rate as the suspension as indicated in Fig. 7(d).

The reason that the "partial inward radial flow" and "pulsing flow" regimes were not observed previously, and that the "outward radial flow" had only been observed at low mass concentra-

8. Regime maps giving the occurrence of flow phenomena as a function of C_m, X_g, and ε for Rotor A. The dashed line gives the maximum power that can be dissipated in the suspension. The points on the graphs indicate observed transitions to partial inward radial flow (○), outward radial flow (□), pulsing flow (△), and cellular flow (●).

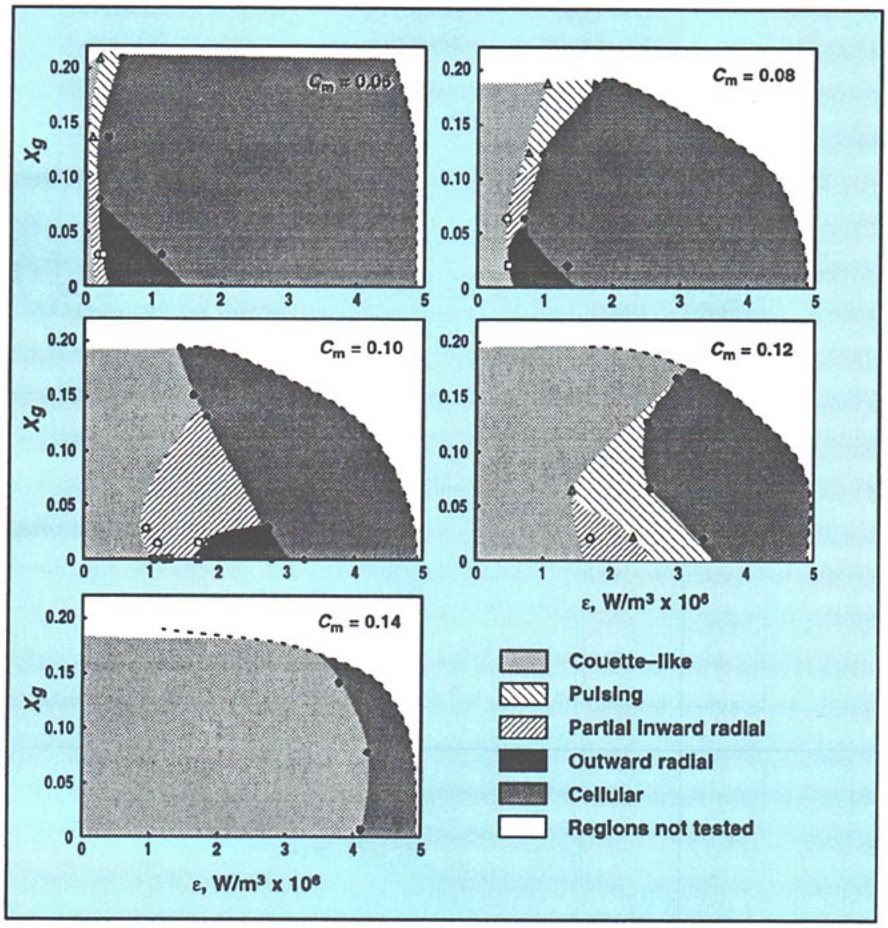

tions, may be due to the method used to obtain and analyze the data in the earlier tests. The experiments conducted with Rotor B used a standard video system having an effective framing rate of only 30–60 pps. This, combined with the more rapid rotor acceleration used in the previous tests (52.4 rad/s^2 vs. 21 rad/s^2) may not have permitted detection of these regimes which, if they existed, would have appeared only as momentary instabilities before the establishment of the more stable flow regimes. The tests with Rotor A were video-taped at 1000 pps and permitted much better resolution of the flow patterns. However, rotor design and suspension gas content ultimately determine the flow regimes possible.

Of the identified flow regimes, only the outward radial and cellular flow regimes maintain complete fiber-suspension motion within the vessel. However, because of the potential for gas accumulation around the rotor noted in the case of the outward flow pattern, the cellular flow pattern would be preferred when gases must be mixed into the suspension. Therefore, it is important to know the conditions under which this regime occurs.

Past investigations have utilized the power dissipation per unit volume to characterize the onset of a fluid-like motion in pulp fiber suspensions (*2, 4*) and this convention is adopted here. **Figure** 8 gives the occurrence of each flow regime as a function of suspension mass concentration, gas void fraction, and power dissipation. The flow regimes encountered in a particular test can be found by following a horizontal line (a given X_g) across the appropriate regime map as the power dissipation is increased. For example, Fig. 8 gives the regime map for a C_m =0.10 FBK suspension. Following the horizontal line corresponding to a gas content of 2% (X_g =0.02) shows that four flow regimes would be encountered in this order: "Couette-like," partial inward radial, outward radial, and cellular flow. Note that neither the extent of radial motion in the "Couette-like" regime nor the vigor of the bulk flow are indicated in these figures. The unshaded areas in these figures represent regions that were not examined ($X_g \geq$ 0.20) or conditions that were not attainable in the shear tester (i.e., above the maximum power dissipation of 4.8×10^6 W/m^3 when X_g =0).

Good fiber-scale mixing is achieved in the cellular flow regime. This was ascertained previously in tests made with Rotor B, in which a small quantity of red-dyed nylon fiber was added to a medium-consistency (C_m =0.10) semibleached kraft pulp suspension (*10*). In these tests, the dyed fiber was placed along the outer wall of the shear tester, the housing packed with pulp, and a test was conducted in which the rotor was ramped from rest to 83 s^{-1} in 10 s. No red fibers were observed in the flow until suspension motion had reached the outer wall of the shear tester. Once the transition to cellular flow had occurred, the dyed fibers became uniformly distributed throughout the suspension in approximately 1.4 s. Examination of individual fiber flocs following the test showed that the red nylon fibers were distributed throughout all flocs, indicating that the flocs must have been disrupted (and therefore that the yield stress of the flocs exceeded) at some point in the flow.

The mixing literature shows that the power dissipation varies greatly within a mixer. In a standard stirred vessel dissipation reaches its maximum close to the rotor tips. Our investigations with the high-speed video showed flocs in the bulk flow of all flow re-

9. Gassed power ratio ($P_g/P_{o,w}$) vs. gas content (X_g) for a FBK suspension mixed with Rotor A at N =75 s^{-1}. The solid curve represents water (C_m =0.0) and is given for comparison.

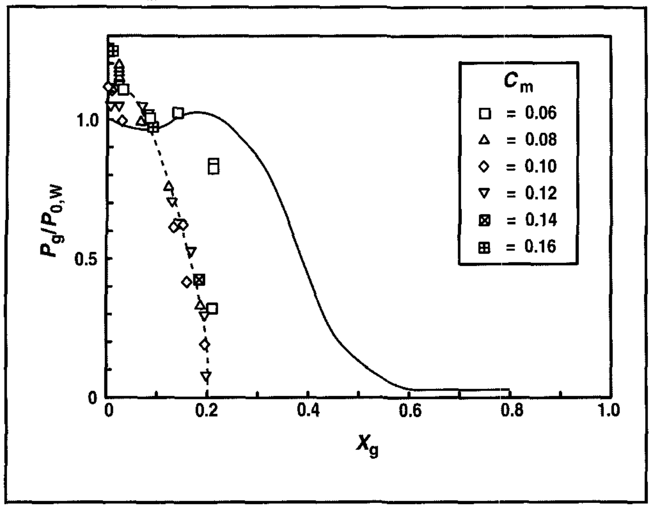

10. Gassed power ratio ($P_g/P_{o,w}$) vs. gas content (X_g) for a FBK suspension mixed with Rotor B at N =75 s^{-1}. The solid curves represent water (C_m =0.0) and are given for comparison.

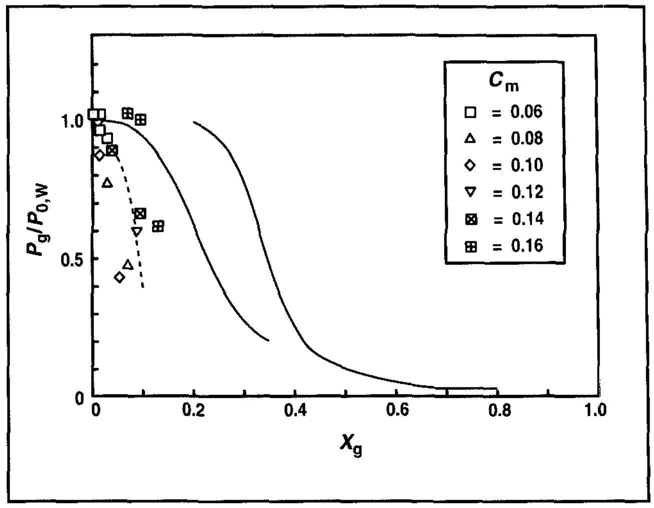

gimes, but in most instances could not resolve flocs adjacent to the rotor. It is in this region where the shear and energy dissipation are highest, and thus where floc disruption is most likely to occur. It is also in this high-shear region where the interfacial area of the gas phase is expected to be developed. Thus good fiber/gas contacting is expected as bubble size is reduced and fiber flocs disrupted. In the flow away from the impeller, rapid floc formation ($<10^{-5}$ s at C_m =0.05) is expected to occur (*11*). The stability of the gas dispersion is unknown and will likely depend on the suspension mass concentration and gas content. Indeed, continued energy expenditure may be necessary to maintain the gas dispersion.

Power used in mixing

The effect of gas content on mixing can also be examined by plotting the gassed power ratio against the gas void fraction. This has been done in **Figs. 9** and **10** for Rotors A and B, respectively. Here, the data obtained for FBK suspensions having mass concentrations between 0.06 and 0.16 have been plotted using the ratio of the power drawn under gassed conditions to that drawn by water under ungassed conditions ($P_g/P_{o,w}$). All data were obtained at a rotor speed of 75 s^{-1}.

When compared with the corresponding water data, the gassed power ratio for the pulp suspensions drops off much more rapidly with increasing gas content. This indicated the formation of large gas cavities and poor gas dispersion.

There is also a large difference in the behavior of the two rotors, and this is related to the quantity of gas that can be accommodated between the rotor vanes, V_v, which is calculated by subtracting the solid volume of the rotor from the total volume swept out by the rotor. For Rotor A (having the deeper vanes), V_v =4.4× 10^{-4} m^3, while Rotor B has V_v =2.2 × 10^{-4} m^3. A high gassed power ratio is maintained only in the vicinity of X_g =0, and in both cases $P_g/P_{o,w}$ reaches 0.5 when $V_g/V_v \approx$ 1.2. However, only suspensions having gas contents less than V_v/V_T can be assured of maintaining some contact between the rotor and suspension under all operating conditions. This effectively places an upper limit on the quantity of gas that can be mixed into the suspension with a given rotor.

Using a $X_g \leq V_v/V_T$ criterion for the test configurations employed here (Fig. 2), Rotor A can handle suspensions containing up to 13% gas by volume, whereas Rotor B is limited to gas contents of less than 7%. However, as we approach these limiting values, the power dissipation, and hence mixing efficiency, drops off.

The energy expended in mixing can also be used to indicate the interfacial area produced. However, unlike the air/water dispersions, it is impossible to observe the gas phase through the opaque fiber suspensions, and thus a correlation of gas "bubble" size with mixer operating conditions is impossible. Indeed, the manner in which the gas phase exists within the suspension is difficult to determine.

Under conditions of "Couette-like" flow, the gas phase migrates to the center of the shear tester. If the gas volume is sufficient to blind the rotor from the suspension, flooding occurs and little or no gas/suspension mixing occurs. If the transition to turbulent motion (i.e., cellular flow) is attained, the gas phase can be mixed throughout the suspension. In most cases, the gas content is fully dispersed and cannot be detected. However, at high gas contents, or in some cases where operating conditions just sustain complete motion, slugs of gas may be seen moving with the bulk flow. This is shown in **Fig. 11**, for a C_m =0.10 FBK suspension mixed with Rotor A where X_g =0.13. Here, although cellular flow has been attained, the energy dissipation is insufficient to maintain all of the gas phase as small, undetectable regions within the suspension. While increasing the energy dissipation should reduce the size of the gas pockets, a 13% volume of gas in suspension is approaching the working capacity of this particular rotor.

Macroscale, fiber-scale, and microscale mixing are all improved as power dissipation within the mixing vessel is increased. However, the introduction of gas to the suspension reduces power dissipation and hence mixing quality. This is attributed to two factors: the impeller losing its ability to effectively transfer momentum to the suspension, and the suspension yield stress, which must be exceeded to maintain fluid-like motion.

The centrifugal forces generated by the impeller tend to segregate the gas phase from the suspension, and the gas phase is drawn to the low-pressure region around the rotor. This accumulation of gas reduces the pumping capacity of the rotor and hence the momentum transferred to the suspension. The separation of gas from the suspension also increases the volumetric concentration of the fibers in the vessel (the suspension is compressed), which increases the yield stress and hence the force that must be applied to maintain motion. Both these factors contribute to the rapid drop in mixing power and the decrease in motion as the gas content of the suspension is increased. Provided the total gas content remains below the critical level ($X_g \leq V_v/V_T$), the impeller will continue to contact the suspension, with the result that some momentum transfer and mixing is possible. However, as shown in **Fig. 12**, once the critical gas content for the rotor is exceeded, very little mixing of the gas phase with the suspension occurs.

The reduction in suspension yield stress as the mass concentration is reduced permits a higher gassed power ratio to be maintained to higher void fractions (see the data for C_m = 0.06 in Fig. 9). However, even in this case, the power level drops off markedly above $X_g \approx 0.20$ due to the formation of a suspension-free zone around the rotor maintained by centrifugal forces. As suspension mass concentration (and hence yield stress) is further reduced, suspension behavior is expected to approach that given by the water curve.

For Newtonian fluids, the rotor power characteristics are given in Fig. 3, which shows that in the turbulent regime (Re ≥ 300), N_p is approximately constant and equal to 3.4 ± 0.6. For pulp suspensions, the effective viscosity of the suspension is unknown. However, the power number for Rotor A—computed for all cases where cellular flow existed and the suspension gas content was less than 1.2 V_v/V_T—was 3.4 ± 0.5. This confirms that a turbulent regime exists and, consequently, that estimates of the rotor speed required to achieve cellular flow can be made using the regime maps (Fig. 8) and the power number:

$$N_p = P/(D^5N^3\rho) \approx \text{constant} \qquad (2)$$

where

P = $2\pi NT$

ε = P/V_T (determined from the regime maps)

N_p = 3.4 plus an acceptable safety factor (to be conservative, one would assume that the impeller was less effective at transferring energy to the suspension, i.e., that N_p was less than 3.4).

Substitution and rearrangement to solve for N gives:

$$N = [(\varepsilon V_T)/(D^5N_p\rho)]^{1/3} \qquad (3)$$

Once the rotational speed is known, the required torque can be computed.

Earlier, we mentioned that both the bulk flow and power dissipation must be taken into account when evaluating the gas-mixing potential of a pulp mixer. This is illustrated by considering the case where a C_m = 0.16 FBK suspension is mixed with Rotor B (see data in Fig. 10). Here a high gassed power ratio is attained even at X_g = 0.10, although motion is confined only to the immediate rotor vicinity. This is due to the friction of the pulp plug against the rotor and demonstrates that the existence of a high $P_g/P_{o,w}$ does not necessarily mean that good mixing is possible. The existence of bulk motion must be ascertained by visual observation or other data (for a known geometry, from regime maps similar to the ones given in Fig. 8). In general, however, when motion does exist throughout the vessel, the larger the power dissipation, the more vigorous is the flow and hence the better is the mixing at the macroscale and the fiber-scale.

Summary and conclusions

For the batch-operated concentric-cylinder mixer geometry studied, the establishment of a turbulent regime that completely fills the vessel is required for effective gas/suspension mixing. The cellular flow regime meets these requirements and can be established within certain operating limits, provided that sufficient power dissipation is maintained. The minimum power requirements were found to depend on both suspension mass concentration and the void fraction occupied by the gas phase. Regime maps were developed for one rotor configuration to identify suitable operating conditions. As with other mixers, increasing power dissipation above the minimum level required will improve both the macroscale and fiber-scale mixing.

When the gas fraction of a suspension is increased, the power that can be imparted by a mixer decreases. This will result in a reduction in mixing quality. Ultimately, a limit is reached beyond which the volume fraction of the gas phase can no longer be increased. For the two mixer geometries studied here, this was found to depend on the volume of gas that could be accommodated by the rotor before it lost contact with the suspension. Here, the gassed power ratio, $P_g/P_{o,w}$, dropped to 0.5 when the suspension gas content reached X_g = 1.2 V_v/V_T, with the power ratio decreasing abruptly at higher gas contents. If one takes $X_g = V_v/V_T$ as indicative of an upper operating limit, in the case of Rotor A, no more than 13% of the suspension volume can be gas. For Rotor B this value drops to 7%. As mixture quality depends to a large degree on the power input, gas limits lower than the maximum would be advised.

These tests were conducted with batch-operated laboratory-scale equipment. However, industrial experience with continuous medium-consistency mixers are consistent with these findings. For example, it is known that the motor load of a medium-consistency mixer drops when the gas flow is turned on or increased. Ultimately, a gas-handling limit is reached beyond which mixing quality suffers. For continuous operation, the drop in mixer load will not be as abrupt as for batch conditions because of the maintenance of suspension flow through the mixer by a pump.

While a mixed three-phase (gas/fiber/water) suspension can be maintained in batch operation by the continued input of power, segregation of the gas phase occurs once the power input has stopped. In continuous operation, an analogous situation occurs once the suspension has passed from the mixer. The stability of the resulting three-phase suspensions have not been assessed, although the need to maintain a stable system will depend on factors such as the bleaching chemistry. For example, the maintenance of a uniform three-phase suspension is more critical when chemical reaction rates are relatively slow. TJ

11. Photographs of a C_m =0.10 FBK suspension with X_g =0.13 ($P_g/P_{o,w}$ =1.02) showing dispersion of the gas phase. Note the motion of a gas pocket, indicated by the arrows in these three images, taken (from top to bottom) at 0, 0.01, and 0.025 s.

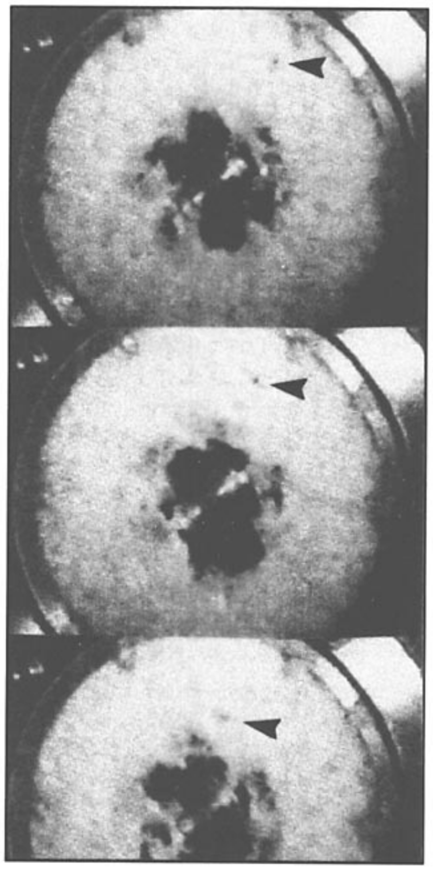

12. Photograph of a C_m =0.12 FBK suspension with X_g =0.20 (N =54.5 s^{-1}) showing the suspension bridging that limits momentum transfer to the bulk of the suspension.

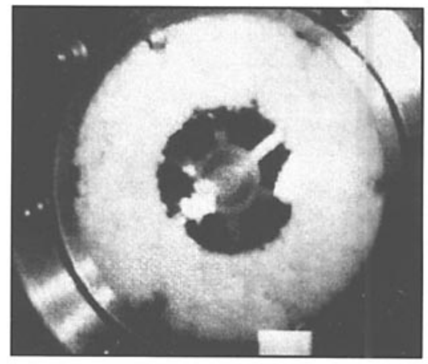

Nomenclature

- C_m = mass fraction of fibers
- d_{10} = bubble diameter, m
- d_{32} = Sauter mean diameter, m
- d_{max} = maximum stable bubble diameter, m
- D = rotor diameter, m
- m_T = total mass, kg
- N = rotation rate, s^{-1}
- N_p = power number, $P/(D^5N^3\rho)$
- P = power, W
- P_g = power drawn when gas is present, W
- P_o = power drawn when gas is not present, W
- $P_{o,w}$ = power drawn when gas is not present, for water, W
- Re = rotor (impeller) Reynolds number, $D^2N\rho/\mu$
- T = torque, N·m
- V_g = gas volume, m^3
- V_v = volume of gas accommodated by rotor, m^3
- V_T = total volume of mixing chamber, m^3
- X_g = volume fraction of gas phase
- ε = power dissipation per unit volume, W/m^3
- ε_m = power dissipated per unit mass, m^2/s^3
- μ = viscosity, Pa·s
- ρ = density, kg/m^3
- ρ_b = bulk density, m_T/V_T, kg/m^3
- ρ_f = density of cellulose, 1500 kg/m^3
- ρ_w = density of water

Literature cited

1. Bennington, C. P. J., Kerekes, R. J., and Grace, J. R., J. Pulp Paper Sci. 15(5): J189(1989).
2. Gullichsen J. and Harkonen, E., Tappi J. 64(6): 69(1981).
3. Bennington, C. P. J., Kerekes, R. J., and Grace, J. R., Can. J. Chem. Eng. 68: 748(1990).
4. Bennington, C. P. J., Kerekes, R. J., and Grace, J. R., Can. J. Chem. Eng. 69: 251(1991).
5. Gray, J. B., "Mixing in agitated vessels," in Mixing: Theory and Practice (V.W. Uhl and J.B. Gray, Eds.), Chap. 4, Academic Press, New York, NY, 1966.
6. Nagata, S., Mixing: Principles and Applications, John Wiley & Sons, Toronto, 1975.
7. Mann, R., Gas-liquid contacting in mixing vessels, Institution of Chemical Engineers, Rugby, England, 1983.
8. Ando, K., Hara, H., and Endoh, K., Intern. Chem. Eng. 11(4): 735(1971).
9. Hinze, J. O., AIChE J. 1(3): 289(1955).
10. Bennington, C. P. J., "Mixing pulp suspensions," Ph.D. thesis, University of British Columbia, Vancouver, BC, 1988.
11. Kerekes, R. J., Soszynski, R. M., and Tam Doo, P. A., "The flocculation of pulp fibers," Transactions of the Eighth Fundamental Research Symposium, Fundamental Research Committee, Oxford, 1: 265(1985).
12. Dosch, J.B., K.M. Singh and T.J. Stenuf, TAPPI 1986 Engineering Conference Proceedings, TAPPI PRESS, Atlanta, p. 721.

The author thanks R. J. Kerekes for valuable comments.

Received for review Dec. 8, 1992.

Accepted Jan. 18, 1993.